Supercooled liquids under shear: Theory and simulation

Kunimasa Miyazaki and David R. Reichman

Department of Chemistry and Chemical Biology, Harvard University, 12 Oxford Street, Cambridge, Massachusetts 02138, USA

Ryoichi Yamamoto

Department of Physics, Kyoto University, Kyoto 606-8502, Japan
and PRESTO, Japan Science and Technology Agency, 4-1-8 Honcho Kawaguchi, Saitama, Japan

We analyze the behavior of supercooled fluids under shear both theoretically and numerically. Theoretically, we generalize the mode-coupling theory of supercooled fluids to systems under stationary shear flow. Our starting point is the set of generalized fluctuating hydrodynamic equations with a convection term. A nonlinear integrodifferential equation for the intermediate scattering function is constructed. This theory is applied to a two-dimensional colloidal suspension. The shear rate dependence of the intermediate scattering function and the shear viscosity is analyzed. We have also performed extensive numerical simulations of a two-dimensional binary liquid with soft-core interactions near, but above, the glass transition temperature. Both theoretical and numerical results show the following. (i) A drastic reduction of the structural relaxation time and the shear viscosity due to shear. Both the structural relaxation time and the viscosity decrease as $\dot{\gamma}^{-\nu}$ with an exponent $\nu \lesssim 1$, where $\dot{\gamma}$ is the shear rate. (ii) Almost isotropic dynamics regardless of the strength of the anisotropic shear flow.

I. INTRODUCTION

Complex fluids such as colloidal suspensions, polymer solutions, and granular fluids exhibit very diverse rheological behavior [1,2]. Shear thinning is among the most well-known phenomena. Such behavior is predicted for simple liquids as well [3,4], but the effect is too small to observe at temperatures well above the glass transition temperature. For supercooled liquids, however, the situation is different. Recently, strong shear thinning behavior was observed by experiments performed on soda-lime silica glasses above the glass transition temperature [5]. Yamamoto *et al.* have done extensive computer simulations of a binary liquid with a soft-core interaction [6] near their glass-transition temperature and found non-Newtonian behavior. The same behavior was found for other systems such as Lennard-Jones mixtures [7,8] and polymer melts [9], too. For all cases, the structural relaxation time and the shear viscosity decrease as $\dot{\gamma}^{-\nu}$, where $\dot{\gamma}$ is the shear rate and ν is an exponent which is less than but close to 1. For such systems driven far from equilibrium, the parameter $\dot{\gamma}$ is not a small perturbation but plays a role similar to an intensive parameter which characterizes the "thermodynamic state" of the system [10]. Such rheological behavior is interesting in its own right, but understanding the dynamics of supercooled liquids in a nonequilibrium state is more important because it has possibilities to shed light on another typical and perhaps more important nonequilibrium problem, namely, that of nonstationary aging. Aging is characterized by slow relaxation after a sudden quench of temperature below the glass transition temperature. In this case, the waiting time plays a similar role to (the inverse of) the shear rate. Aging behavior has been extensively studied in spin glasses (see Ref. [11], and references therein). Aging is also observed in structural glasses [12]. There have been recent attempts to study the aging of struc-

tural glasses theoretically [13] but no analysis and comparison to experiments or simulation results [12] have been presented due to the complicated nonstationary nature of the problem.

The relationship between aging and a driven, steady-state system was considered using a schematic model based on the exactly solvable *p*-spin spin glass by Berthier, Barrat, and Kurchan [14]. This theory naturally gives rise to effective temperatures. The validity of their idea was tested numerically for supercooled liquids [7]. There have also been attempts to observe aging by exerting shear on the system instead of quenching the temperature [15]. Recently, there have been attempts to develop the mode-coupling theory for the sheared glasses [16,17]. Fuchs and Cates have developed the mode-coupling theory for the sheared colloidal suspensions using projection operator techniques [17]. They have analyzed a closed equation for the correlation function for a schematic model where the shear is exerted on all direction equally ("the isotropically sheared hard sphere model"). In their model, shear is turned on at the initial time and therefore the dynamics are genuinely nonstationary.

In this paper, we investigate the dynamics of supercooled fluids under shear both theoretically and numerically for a realistic system. We extend the standard mode-coupling theory (MCT) for supercooled fluids and compare the solutions with the numerical simulation results. We mainly focus on the microscopic origin of the rheological behavior. The relationship with the more generic aging problem will not be discussed here. Since our goal is the investigation of shear thinning behavior, we have neglected violations of the fluctuation-dissipation theorem. We start with generalized fluctuating hydrodynamic equations with a convection term. Using several approximations, we obtain a closed nonlinear equation for the intermediate scattering function for the sheared system. The theory is applicable to both normal liq-

uids and colloidal suspensions in the absence of hydrodynamic interactions. Similar approach has been applied to the self-diffusion of the hard sphere colloidal suspension at relatively low densities by Indrani *et al.* [18]. Extensive computer simulations are implemented for a two-dimensional binary liquid interacting with soft-core interactions. The effects of shear on microscopic structure, the structural relaxation time, and rheological behavior are discussed. Results both from the theory and the simulation show good qualitative agreement despite the differences between the systems considered. Special attention is paid to the directional dependence of the structural relaxation.

The paper is organized as follows. In the next section, we develop the MCT for sheared suspensions. Complexities which do not exist in mean-field spin glass models and how those complexities should be treated are elucidated here. A possible way to explore the situation without invoking the fluctuation-dissipation theorem is also discussed. In Sec. III, the model and our simulation method are explained. The results both from theory and simulation are discussed in Sec. IV. In Sec. V we conclude.

II. MODE-COUPLING THEORY

We shall consider a two-dimensional colloidal suspension under a stationary shear flow given by

$$\mathbf{v}_0(\mathbf{r}) = \mathbf{\Gamma} \cdot \mathbf{r} = (\dot{\gamma}y, 0), \tag{2.1}$$

where $\dot{\gamma}$ is the shear rate and $(\mathbf{\Gamma})_{\alpha\beta} = \dot{\gamma}\delta_{\alpha x}\delta_{\beta y}$ is the velocity gradient matrix. Generalization to higher dimensions is trivial. We start with the generalized fluctuating hydrodynamic equations [19,20]. This is a natural generalization of the fluctuating hydrodynamics developed by Landau and Lifshitz [21] to short wavelengths where the intermolecular correlations become important. Fluctuating fields for the number density $\rho(\mathbf{r}, t)$ and the velocity $\mathbf{v}(\mathbf{r}, t)$ of the colloidal suspension obey the following set of nonlinear Langevin equations:

$$\frac{\partial \rho}{\partial t} = -\nabla \cdot (\rho \mathbf{v}),$$

$$m\frac{\partial (\rho \mathbf{v})}{\partial t} + m\nabla \cdot (\rho \mathbf{v} \cdot \mathbf{v}) = -\rho \nabla \frac{\delta \mathcal{F}}{\delta \rho} - \zeta_0 \rho(\mathbf{v} - \mathbf{v}_0) + \mathbf{f}_R,$$

$$\tag{2.2}$$

where m is the mass of a single colloidal particle, $\mathcal{F}$ is the free energy of the system, and ζ_0 is a bare collective friction coefficient for colloidal particles. ζ_0 has a weak density and distance dependence due to hydrodynamic interactions [22] but we shall neglect these effects. The friction term is specific for the colloidal case. In the case of liquids, it should be replaced by a stress term which is proportional to the gradient of the velocity field multiplied by the shear viscosity. Both cases, however, lead to the same dynamical behavior on the long time scales which are of interest here. $\mathbf{f}_R(\mathbf{r}, t)$ is the random force which satisfies the fluctuation-dissipation theorem (FDT) of the second kind [23,50]

$$\langle f_{R,i}(\mathbf{r},t) f_{R,j}(\mathbf{r}',t') \rangle_0 = 2k_B T \rho(\mathbf{r},t) \zeta_0 \delta_{ij} \delta(\mathbf{r} - \mathbf{r}') \delta(t - t') \tag{2.3}$$

for $t \geq t'$, where $\langle \cdots \rangle_0$ is an average over the conditional probability for a fixed value of $\rho(\mathbf{r}, t)$ at $t = t'$. Note that the random force depends on the density and thus the noise is multiplicative. This fact makes a mode-coupling analysis more involved as we discuss later in this section. We assume that the second FDT holds even in nonequilibrium state since the correlation of the random forces are short ranged and short lived, and thus the effect of the shear is expected to be negligible. The first term on the right-hand side of the equation for the momentum is the osmotic pressure term. Here we assume that the free energy $\mathcal{F}$ is well approximated by that of the equilibrium form and is given by the well-known expression

$$\beta\mathcal{F} \simeq \int d\mathbf{r} \, \rho(\mathbf{r})\{\ln \rho(\mathbf{r})/\rho_0 - 1\}$$

$$-\frac{1}{2}\int d\mathbf{r}_1 \int d\mathbf{r}2 \, \delta\rho(\mathbf{r}_1)c(r_{12})\delta\rho(\mathbf{r}_2), \tag{2.4}$$

where $\beta = 1/k_B T$, ρ_0 is the average density, and $c(r)$ is the direct correlation function. We have neglected correlations of more than three points, such as the triplet correlation function $c_3(\mathbf{r}_1, \mathbf{r}_2, \mathbf{r}_3)$, whose effect becomes important for the fluids with stronger directional interactions such as silica [24]. Under shear, it is expected that $c(r)$ will be distorted and should be replaced by a nonequilibrium steady state form $c_{\text{NE}}(\mathbf{r})$, which is an anisotropic function of $\mathbf{r}$. It is, however, natural to expect that this distortion is small on the molecular length scales which play the most important role in the slowing down of structural relaxation near the glass transition. The distortion of the structure under shear is given up to linear order in the shear rate by [25]

$$S_{\text{NE}}(\mathbf{k}) = S(k)\left\{ 1 + \frac{\hat{\mathbf{k}} \cdot \mathbf{\Gamma} \cdot \hat{\mathbf{k}}}{2kD_0}\frac{dS(k)}{dk} \right\}, \tag{2.5}$$

where $S(k)$ and $S_{\text{NE}}(\mathbf{k})$ is the static structure factor in the absence and in the presence of the shear, respectively. $D_0 = k_B T/\zeta_0$ is the diffusion coefficient in the dilute limit $k \equiv |\mathbf{k}|$ and $\hat{\mathbf{k}} \equiv \mathbf{k}/|\mathbf{k}|$. The direct correlation function in the Fourier representation of $c(r)$ is related to the structure factor by $nc(k) = 1 - 1/S(k)$. From Eq. (2.5), we find that the distortion due to the shear is characterized by the Péclet number defined by $\text{Pe} = \dot{\gamma}\sigma^2/D_0$, where σ is the diameter of the particle. Hereafter we shall neglect the distortion and use the direct correlation function at equilibrium, assuming the Péclet number is very small.

We linearize Eq. (2.2) around the stationary state as $\rho = \rho_0 + \delta\rho$ and $\mathbf{v} = \mathbf{v}_0 + \delta\mathbf{v}$, where ρ_0 is the average density. Transforming to wave vector space, we obtain the following equations:

$$\left(\frac{\partial}{\partial t} - \mathbf{k} \cdot \mathbf{\Gamma} \cdot \frac{\partial}{\partial \mathbf{k}} \right)\delta\rho_{\mathbf{k}}(t) = \frac{ik}{m}J_{\mathbf{k}}(t),$$

$$\left(\frac{\partial}{\partial t} - \mathbf{k} \cdot \mathbf{\Gamma}\frac{\partial}{\partial \mathbf{k}} + \hat{\mathbf{k}} \cdot \mathbf{\Gamma} \cdot \hat{\mathbf{k}}\right)J_{\mathbf{k}}(t) = -\frac{ik}{\beta S(k)}\delta\rho_{\mathbf{k}}(t)$$

$$-\frac{1}{m\beta}\int_{\mathbf{q}} i\hat{\mathbf{k}} \cdot \mathbf{q}c(q)\delta\rho_{\mathbf{k}-\mathbf{q}}(t)\delta\rho_{\mathbf{q}}(t) - \frac{\zeta_0}{m}J_{\mathbf{k}}(t) + f_{R\mathbf{k}}(t),$$

(2.6)

where $J_{\mathbf{k}}(t) = m\rho_0\hat{\mathbf{k}} \cdot \delta\mathbf{v}_{\mathbf{k}}(t)$ is the longitudinal momentum fluctuation, and $\int_{\mathbf{q}} \equiv \int d\mathbf{q}/(2\pi)^2$. We have neglected the quadratic terms proportional to $\mathbf{J}_{\mathbf{q}}\mathbf{J}_{\mathbf{k}-\mathbf{q}}$. Note that Eq. (2.6) does not contain coupling to transverse momentum fluctuations even in the presence of shear.

The direct numerical integration of Eq. (2.6) is in principle possible but it is expensive and not theoretically enlightening [26]. Rather we shall construct the approximated closure for the correlation functions, a so-called mode-coupling approximation [27–29]. There are several approaches to derive mode-coupling equations, including the use of the Mori-Zwanzig projection operator and a decoupling approximation [27], or implementation of a loop expansion developed in the context of the equilibrium critical phenomena and generalized to the dynamic case [29,30]. Both approaches lead to essentially the same equations if the system is at equilibrium. Under nonequilibrium conditions, however, the loop expansion approach is more straightforward and flexible. We shall adopt the loop expansion approach to the nonlinear Langevin equation with both multiplicative noise and the full convection term. Equation (2.6) can be cast to a general form of the nonlinear Langevin equation written as

$$\frac{dx_i}{dt} = \mu_{ij}x_j + \frac{1}{2}\mathcal{V}_{ijk}x_jx_k + f_{R,i},$$

(2.7)

where $\mathbf{x}(t) = [\delta\rho_{\mathbf{k}}(t), J_{\mathbf{k}}(t)]$ is a field variable, μ_{ij} is the linear coefficient matrix, and the nonlinear coupling coefficient $\mathcal{V}_{ijk}$ is the vertex tensor which satisfies the symmetric relation $\mathcal{V}_{ijk} = \mathcal{V}_{ikj}$. Finally, $f_{R,i}(t)$ is the random force field which satisfies the second FDT,

$$\langle f_{R,i}(t)f_{R,j}(t')\rangle_0 = k_B L_{ij}(\mathbf{x})\delta(t - t'),$$

(2.8)

where $L_{ij}(\mathbf{x})$ is the $\mathbf{x}$-dependent Onsager coefficient which is to be expanded to the lowest order as

$$L_{ij}(\mathbf{x}) = L_{ij}^{(0)} + L_{ij,k}^{(1)}x_k,$$

(2.9)

where $L_{ij,k}^{(1)} \equiv \partial L_{ij}(\mathbf{x})/\partial x_k|_{\mathbf{x}=0}$. Comparing Eq. (2.7) with Eq. (2.6), the elements of the linear coefficient matrix are given by

$$\mu_{\rho_{\mathbf{k}}\rho_{\mathbf{k}'}} = \mathbf{k} \cdot \mathbf{\Gamma} \cdot \frac{\partial}{\partial \mathbf{k}}\delta_{\mathbf{k},\mathbf{k}'},$$

$$\mu_{\rho_{\mathbf{k}}J_{\mathbf{k}'}} = \frac{ik}{m}\delta_{\mathbf{k},\mathbf{k}'},$$

$$\mu_{J_{\mathbf{k}}\rho_{\mathbf{k}'}} = \frac{ik}{\beta S(k)}\delta_{\mathbf{k},\mathbf{k}'},$$

$$\mu_{J_{\mathbf{k}}J_{\mathbf{k}'}} = \left(\mathbf{k} \cdot \mathbf{\Gamma} \cdot \frac{\partial}{\partial \mathbf{k}} - \hat{\mathbf{k}} \cdot \mathbf{\Gamma} \cdot \hat{\mathbf{k}}\right)\delta_{\mathbf{k},\mathbf{k}'} - \frac{\zeta_0}{m}\delta_{\mathbf{k},\mathbf{k}'}.$$

(2.10)

Nonzero elements of the vertex tensor are given by

$$\mathcal{V}_{J_{\mathbf{k}}\rho_{\mathbf{k}'}\rho_{\mathbf{k}''}} = -\frac{1}{\beta V}\{i\hat{\mathbf{k}} \cdot \mathbf{k}'c(\mathbf{k}') + i\hat{\mathbf{k}} \cdot \mathbf{k}''c(\mathbf{k}'')\}\delta_{\mathbf{k},\mathbf{k}'+\mathbf{k}''},$$

(2.11)

where V is the volume of the system. Finally,

$$L_{J_{\mathbf{k}}J_{\mathbf{k}'}}^{(0)} = \zeta_0\rho_0 TV\delta_{\mathbf{k},-\mathbf{k}'}$$

$$L_{J_{\mathbf{k}}J_{\mathbf{k}'},\rho_{\mathbf{k}''}}^{(1)} = T\zeta_0\delta_{\mathbf{k}+\mathbf{k}',\mathbf{k}''}.$$

(2.12)

All other components are zero. In the above expressions,

$$\delta_{\mathbf{k},\mathbf{k}'} \equiv \frac{(2\pi)^2}{V}\delta(\mathbf{k} - \mathbf{k}')$$

is the Dirac delta function. We construct the closure equation for the correlation function $C_{ij}(t,t') = \langle x_i(t)x_j(t')\rangle$. Since we are treating the stationary state, the time translation invariance holds and, thus, $C_{ij}(t,t') = C_{ij}(t-t')$. A general scheme for the loop expansion method for the Langevin equation with multiplicative noise has been discussed by Phythian [31]. Up to one loop, the equation for the correlation function is written as [32]

$$\frac{dC_{ij}(t-t')}{dt} - \mu_{i\alpha}C_{\alpha j}(t-t') - 2k_B L_{i\alpha}^{(0)}\hat{G}_{\alpha j}^{\dagger}(t-t')$$

$$= \int_{-\infty}^{t} dt_1\sum_{i\alpha}(t-t_1)C_{\alpha j}(t_1-t') + \int_{-\infty}^{t'} dt_1\, D_{i\alpha}(t-t_1)$$

$$\times \hat{G}_{\alpha j}^{\dagger}(t_1-t')\frac{d\hat{G}_{ij}(t-t')}{dt} - \mu_{i\alpha}\hat{G}_{\alpha j}(t-t')$$

$$= \delta_{ij}\delta(t-t') + \int_{t'}^{t} dt_1\sum_{i\alpha}(t-t_1)\hat{G}_{\alpha j}(t_1-t') \quad (2.13)$$

with the memory kernels defined by

$$\sum_{ij}(t) = \mathcal{V}_{i\alpha\beta}\hat{G}_{\alpha\lambda}(t)C_{\beta\mu}(t)\mathcal{V}_{\lambda\mu j} + k_B\mathcal{V}_{i\alpha\beta}\hat{G}_{\alpha\lambda}(t)\hat{G}_{\beta\mu}(t)L_{\lambda\mu,j}^{(1)},$$

$$D_{ij}(t) = \frac{1}{2}\mathcal{V}_{i\alpha\beta}C_{\alpha\lambda}(t)C_{\beta\mu}(t)\mathcal{V}_{j\lambda\mu} + 2k_B\mathcal{V}_{i\alpha\beta}\hat{G}_{\alpha\lambda}(t)C_{\beta\mu}(t)L_{j\lambda,\mu}^{(1)}$$

$$+ 2k_B L_{i\alpha,\beta}^{(1)}\hat{G}_{\alpha\lambda}^{\dagger}(t)C_{\beta\mu}(t)\mathcal{V}_{j\lambda,\mu}.$$

(2.14)

In these expressions, we have introduced the propagator defined by

$$\hat{G}_{ij}(t-t') = \left\langle\frac{\delta x_i(t)}{\delta f_{R,j}(t')}\right\rangle.$$

(2.15)

$\hat{G}_{ij}^{\dagger}(t-t') \equiv \hat{G}_{ji}(t'-t)$ is the conjugate of the propagator. Equation (2.13) together with Eq. (2.14) are so-called mode-coupling equations.

Without further assumption, one needs to solve the coupled equation for the correlation function and the propagator. The propagator can be eliminated, however, if the fluctuation-dissipation theorem of the first kind (first FDT) is valid. The first FDT relates the correlation function to the response function $\chi_{ij}(t)$ via the equation

$$\chi_{ij}(t) = -\frac{\theta(t)}{k_B T}\frac{dC_{ij}(t)}{dt}, \qquad (2.16)$$

where $\theta(t)$ is the heaviside function. Note that the response function $\chi_{ij}(t)$ is generally neither the same as, nor proportional to, the propagator $\hat{G}_{ij}(t)$. $\chi_{ij}(t)$ represents the response of the system to the perturbation via external fields or through the boundary, whereas $\hat{G}_{ij}(t)$ represents the response to a random force field. If the Langevin equation is linear, both are the same, but this is not true in general for the nonlinear Langevin equation. To one loop, to be consistent with the mode-coupling approximation, the response function is written as [32,33]

$$\chi_{ij}(t-t') = \frac{1}{T}\hat{G}_{ik}(t-t')\{\boldsymbol{M}^{(0)}+\boldsymbol{L}^{(0)}\}_{kj} + \frac{1}{T}\int dt_1\, \hat{G}_{ik}(t-t_1)$$
$$\times \mathcal{V}_{k\alpha\beta}\hat{G}_{\alpha\lambda}(t_1-t')C_{\beta\mu}(t_1-t')\{\boldsymbol{M}^{(1)}+\boldsymbol{L}^{(1)}\}_{\lambda j,\mu}, \qquad (2.17)$$

where the tensors $M_{ij}^{(0)}$ and $M_{ij,k}^{(1)}$ are defined by $M_{ij}(\mathbf{x}) \simeq M_{ij}^{(0)}+M_{ij,k}^{(1)}x_k$. $M_{ij}(\mathbf{x})$ is the matrix which is defined by the reversible part of the nonlinear Langevin equation. In general, we can express the Langevin equation as

$$\frac{dx_i}{dt} = v_i(\mathbf{x}) + M_{ij}(\mathbf{x})\frac{\delta S}{\delta x_j} + L_{ij}(\mathbf{x})\frac{\delta S}{\delta x_j} + f_{R,i}, \qquad (2.18)$$

where S is the entropy of the whole system and $v_i(\mathbf{x})$ is a term which originates from the nonequilibrium constraint such as the convection for the sheared system. From this definition, the reversible term does not contribute to the entropy production and thus the matrix $M_{ij}(\mathbf{x})$ is antisymmetric. For the system considered here, the nonzero elements are given by

$$M_{\rho_{\mathbf{k}}J_{\mathbf{k}'}} = -M_{J_{\mathbf{k}'}\rho_{\mathbf{k}}} = -ikT(\rho_0 V\delta_{\mathbf{k},-\mathbf{k}'} + \delta\rho_{\mathbf{k}+\mathbf{k}'}). \quad (2.19)$$

If the system is in equilibrium, one may eliminate the propagator in favor of the correlation function in Eq. (2.13) by using the first FDT, Eq. (2.16) [32,34,35]. If the system is out of equilibrium, one has to solve the coupled equations (2.13). For the case of the p-spin-glass model with an external drive, Berthier *et al.* have analyzed the equation similar Eq. to (2.13) [14]. They have found that there is a systematic deviation from the first FDT which is reminiscent of violations of FDT that occur during aging. Extensive computer simulation supports these results [7]. A similar analysis for real fluids is necessary but it is inevitably more involved due to the complicated tensorial nature of the nonlinear coupling. In this paper, we shall not focus on the fundamental problem of the validity of the fluctuation-dissipation theorem and assume that the first FDT is valid. We shall show that even

with this simplification, the theory can explain qualitative several aspects of the dynamical behavior very well. Using the first FDT, as in equilibrium case, one can eliminate $\hat{G}_{ij}(t)$ from Eq. (2.13) and the final expression is given by [32]

$$\frac{dC_{ij}(t-t')}{dt} - \mu_{ik}C_{kj}(t-t') - 2k_B L_{ik}^{(0)}\hat{G}_{kj}^{\dagger}(t-t')$$
$$= \int_{t'}^{t} dt_1\, M_{ik}(t-t_1)C_{kj}(t_1-t') \qquad (2.20)$$

with the memory kernel given by

$$M_{ij}(t) = -\frac{1}{2}\mathcal{V}_{i\alpha\beta}C_{\alpha\lambda}(t)C_{\beta\mu}(t)\{\mathcal{V}_{k\lambda\mu} - 2\mathcal{L}_{k\lambda\mu}\}C_{kj}^{-1}(0). \qquad (2.21)$$

These equations are almost identical to the conventional mode-coupling equations [34,35] except for $(-2\mathcal{L}_{k\lambda\mu})$ term which appears in the vertex term of the memory kernel. The third term on the left-hand side of Eq. (2.20) enters naturally to guarantee the time-reversal symmetry of the correlation function. $\mathcal{L}_{ijk}$ is defined by

$$\mathcal{L}_{ijk} \equiv L_{i\alpha}^{(0)}S_{\alpha jk}^{(3)} + L_{i\alpha,j}^{(1)}S_{\alpha k}^{(2)} + L_{i\alpha,k}^{(1)}S_{\alpha j}^{(2)}, \qquad (2.22)$$

where we have defined $S_{ij}^{(2)}$ and $S_{ijk}^{(3)}$ by

$$S_{ij}^{(2)} \equiv \left.\frac{\partial^2 S}{\partial x_i\,\partial x_j}\right|_{\mathbf{x}=0} \quad\text{and}\quad S_{ijk}^{(3)} \equiv \left.\frac{\partial^3 S}{\partial x_i\,\partial x_j\,\partial x_k}\right|_{\mathbf{x}=0}. \qquad (2.23)$$

The term $(-2\mathcal{L}_{k\lambda\mu})$ is a new term which originates from the multiplicative noise. Since the density- and velocity-dependent part of the entropy is given by

$$S = \int d\mathbf{r}\frac{J^2(\mathbf{r})}{2T\rho(\mathbf{r})} + \frac{1}{T}\mathcal{F}, \qquad (2.24)$$

$S_{ij}^{(2)}$ and $S_{ijk}^{(3)}$ are given by

$$S_{J_{\mathbf{k}}J_{\mathbf{k}'}}^{(2)} = -\frac{1}{m\rho_0 TV}\delta_{\mathbf{k},-\mathbf{k}'},$$

$$S_{\rho_{\mathbf{k}}\rho_{\mathbf{k}'}}^{(2)} = -\frac{k_B}{\rho_0 S(k)V}\delta_{\mathbf{k},-\mathbf{k}'},$$

$$S_{\rho_{\mathbf{k}}\rho_{\mathbf{k}'}\rho_{\mathbf{k}''}}^{(3)} = \frac{k_B}{\rho_0^2 V^2}\delta_{\mathbf{k}+\mathbf{k}'+\mathbf{k}'',0},$$

$$S_{J_{\mathbf{k}}J_{\mathbf{k}'}\rho_{\mathbf{k}''}}^{(3)} = \frac{1}{m\rho_0^2 TV^2}\delta_{\mathbf{k}+\mathbf{k}'+\mathbf{k}'',0}. \qquad (2.25)$$

Combining this with Eq. (2.12), we find that $\mathcal{L}_{ijk}=0$ for all elements. Therefore, the final expression for the mode-coupling equation in the present case becomes equivalent with the conventional one [27]. Note that the situation will change if we consider different physical situation: For example, if we start with the diffusion equation, which is obtained in the overdamped limit of Eq. (2.6), $\mathcal{L}_{ijk}$ plays an essential role [36].

Now let us substitute all matrix elements given by Eqs. (2.10) and (2.11) to Eq. (2.20), we have the set of equations given by

$$\left(\frac{\partial}{\partial t} - \mathbf{k} \cdot \mathbf{\Gamma} \cdot \frac{\partial}{\partial \mathbf{k}}\right) C_{\rho_{\mathbf{k}}\rho_{\mathbf{k'}}}(t) = -ikC_{J_{\mathbf{k}}\rho_{\mathbf{k'}}}(t),$$

$$\left(\frac{\partial}{\partial t} - \mathbf{k} \cdot \mathbf{\Gamma} \cdot \frac{\partial}{\partial \mathbf{k}} - \hat{\mathbf{k}} \cdot \mathbf{\Gamma} \cdot \hat{\mathbf{k}}\right) C_{J_{\mathbf{k}}\rho_{\mathbf{k'}}}(t)$$

$$= -\frac{ik}{m\beta S(k)} C_{\rho_{\mathbf{k}}\rho_{\mathbf{k'}}}(t) - \frac{\zeta_0}{m} C_{J_{\mathbf{k}}\rho_{\mathbf{k'}}}(t)$$

$$- \frac{1}{m}\int_0^t dt_1 \sum_{\mathbf{k''}} \delta\zeta(\mathbf{k},\mathbf{k''},t-t_1) C_{J_{\mathbf{k''}}\rho_{\mathbf{k'}}}(t_1),$$

(2.26)

where

$$\sum_{\mathbf{k}} \equiv \frac{V}{(2\pi)^2}\int d\mathbf{k}.$$

(2.27)

The memory kernel $\delta\zeta(\mathbf{k},\mathbf{k'},t)$ is given by

$$\delta\zeta(\mathbf{k},\mathbf{k'},t) = \frac{m}{2} \sum_{\mathbf{q}_1} \sum_{\mathbf{q}_2} \sum_{\mathbf{p}_1} \sum_{\mathbf{p}_2} \sum_{\mathbf{k''}} \mathcal{V}_{J_{\mathbf{k}}\rho_{\mathbf{q}_1}\rho_{\mathbf{q}_2}} C_{\rho_{\mathbf{q}_1}\rho_{\mathbf{p}_1}}(t) C_{\rho_{\mathbf{q}_2}\rho_{\mathbf{p}_2}}(t)$$

$$\times \mathcal{V}_{J_{\mathbf{k''}}\rho_{\mathbf{p}_1}\rho_{\mathbf{p}_2}} C^{-1}_{J_{\mathbf{k''}}J_{\mathbf{k'}}}(0)$$

$$= \frac{\beta}{2n\mathcal{V}} \sum_{\mathbf{q}} \sum_{\mathbf{p}} V_{J_{\mathbf{k}}\rho_{\mathbf{q}}\rho_{\mathbf{k}-\mathbf{q}}} C_{\rho_{\mathbf{q}}\rho_{\mathbf{p}}}(t) C_{\rho_{\mathbf{k}-\mathbf{q}}\rho_{-\mathbf{k'}-\mathbf{p}}}(t)$$

$$\times \mathcal{V}_{J_{-\mathbf{k'}}\rho_{\mathbf{p}}\rho_{-\mathbf{k'}-\mathbf{p}}} = \frac{1}{2n^2N\beta}\int_{\mathbf{q}}\int_{\mathbf{p}} V_{\mathbf{k}}(\mathbf{q},\mathbf{k}$$

$$-\mathbf{q}) C_{\rho_{\mathbf{q}}\rho_{-\mathbf{p}}}(t) C_{\rho_{\mathbf{k}-\mathbf{q}}\rho_{-\mathbf{k'}+\mathbf{p}}}(t) V_{\mathbf{k'}}(\mathbf{p},\mathbf{k'}-\mathbf{p}),$$

(2.28)

where N is the total number of the particles in the system and we have defined the vertex function

$$V_{\mathbf{k}}(\mathbf{q},\mathbf{k}-\mathbf{q}) = \hat{\mathbf{k}}\cdot\mathbf{q}nc(q) + \hat{\mathbf{k}}\cdot(\mathbf{k}-\mathbf{q})nc(|\mathbf{k}-\mathbf{q}|).$$

(2.29)

In the derivation of Eq. (2.28), we have used the momentum equal-time correlation function given by

$$C_{J_{\mathbf{k}}J_{\mathbf{k'}}}(0) = \frac{mnV}{\beta}\delta_{\mathbf{k},-\mathbf{k'}}.$$

(2.30)

If the system is in equilibrium, time and space translational invariance is satisfied and the correlation function becomes $C_{\alpha(\mathbf{r})\beta(\mathbf{r'})}(t) = C_{\alpha(\mathbf{r}-\mathbf{r'})\beta(0)}(t)$ or, in $\mathbf{k}$ space, $C_{\alpha_{\mathbf{k}}\beta_{\mathbf{k'}}}(t) = C_{\alpha_{\mathbf{k}}\beta_{-\mathbf{k}}}(t) \times \delta_{\mathbf{k},-\mathbf{k'}}$. In the presence of shear, however, this should be modified as [37]

$$C_{\alpha(\mathbf{r})\beta(\mathbf{r'})}(t) = C_{\alpha(\mathbf{r}-\mathbf{r'}(t))\beta(0)}(t),$$
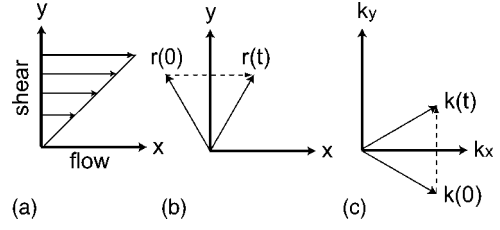
(2.31)

where we defined the time-dependent position vector by

FIG. 1. (a) Geometry of shear flow. (b) Shear advection in real space. (c) Shear advection in Fourier space.

$$\mathbf{r}(t) \equiv \exp[\mathbf{\Gamma}t]\cdot\mathbf{r} = \mathbf{r} + \dot{\gamma}ty\hat{\mathbf{e}}_x,$$

(2.32)

where $\hat{\mathbf{e}}_x$ is an unit vector oriented along the x axis. In wave vector space, this is expressed as

$$C_{\alpha_{\mathbf{k}}\beta_{\mathbf{k'}}}(t) = C_{\alpha_{\mathbf{k}(t)}\beta_{-\mathbf{k}}}(t) \times \delta_{\mathbf{k}(t),-\mathbf{k'}} = C_{\alpha_{\mathbf{k'}(t)}\beta_{\mathbf{k}}}(t) \times \delta_{\mathbf{k},-\mathbf{k'}(-t)}$$

(2.33)

with the time-dependent wave vector defined by

$$\mathbf{k}(t) = \exp[{}^t\mathbf{\Gamma}t]\cdot\mathbf{k} = \mathbf{k} + \dot{\gamma}tk_x\hat{\mathbf{e}}_y,$$

(2.34)

where ${}^t\mathbf{\Gamma}$ denotes the transpose of $\mathbf{\Gamma}$. Figure 1(b) shows how the shear flow advects a positional vector $\mathbf{r}$ by Eq. (2.32) in a time interval of duration t. The corresponding time-dependent wave vector, (2.34), is shown in Fig. 1(c). Equations (2.31) and (2.33) state that the fluctuations satisfy translational invariance in a reference frame flowing with the shear contours. Using this property, Eq. (2.28) becomes

$$\delta\zeta(\mathbf{k},\mathbf{k'},t) = \frac{1}{2\rho_0^2N\beta}\int_{\mathbf{q}}\int_{\mathbf{p}} V_{\mathbf{k}}(\mathbf{q},\mathbf{k}-\mathbf{q}) C_{\rho_{\mathbf{q}}\rho_{-\mathbf{q}(t)}}$$

$$\times (t) C_{\rho_{\mathbf{k}-\mathbf{q}}\rho_{-\mathbf{k}(t)+\mathbf{q}(t)}}(t) V_{\mathbf{k}(t)}(\mathbf{p}(t),\mathbf{k}(t)$$

$$-\mathbf{q}(t))\delta_{\mathbf{p},\mathbf{q}(t)}\delta_{\mathbf{k'},\mathbf{k}(t)} = \frac{1}{2\rho_0^2NV\beta}\int_{\mathbf{q}} V_{\mathbf{k}}(\mathbf{q},\mathbf{k}$$

$$-\mathbf{q}) C_{\rho_{\mathbf{q}}\rho_{-\mathbf{q}(t)}}(t) C_{\rho_{\mathbf{k}-\mathbf{q}}\rho_{-\mathbf{k}(t)+\mathbf{q}(t)}}(t) V_{\mathbf{k}(t)}(\mathbf{p}(t),\mathbf{k}(t)$$

$$-\mathbf{q}(t))\delta_{\mathbf{k'},\mathbf{k}(t)} \equiv \delta\zeta(\mathbf{k},t) \times \delta_{\mathbf{k'},\mathbf{k}(t)}.$$

(2.35)

Introducing the intermediate scattering function by

$$F(\mathbf{k},t) \equiv \frac{1}{N}C_{\rho_{\mathbf{k}(-t)}\rho_{-\mathbf{k}}}(t) = \frac{1}{N}\langle\delta\rho_{\mathbf{k}(-t)}(t)\delta\rho_{-\mathbf{k}}(0)\rangle,$$

(2.36)

$\delta\zeta(\mathbf{k},t)$ can be rewritten as

$$\delta\zeta(\mathbf{k},t) = \frac{1}{2\rho_0\beta}\int_{\mathbf{q}} V_{\mathbf{k}}(\mathbf{q},\mathbf{k}-\mathbf{q})F(\mathbf{q}(t),t)F(\mathbf{k}(t)-\mathbf{q}(t),t)$$

$$\times V_{\mathbf{k}(t)}(\mathbf{p}(t),\mathbf{k}(t)-\mathbf{q}(t)),$$

(2.37)

This is the memory kernel in the presence of the shear. This has exactly the same structure as the equilibrium one [27] except for the time dependence appearing on the wave vectors. The physical interpretation of Eq. (2.37) is simple: The memory kernel has the general structure of two correlation functions sandwiched by two vertex functions. This means

that the interactions of two fluctuations with modes $\mathbf{q}$ and $\mathbf{k}-\mathbf{q}$ scatter at a certain time and then propagate freely in a "mean field" and after a time t, they recollide and interact. Under shear, however, by the time the second interactions take place, the fluctuations are streamed away by the flow.

We also define the cross correlation function

$$H(\mathbf{k},t) \equiv \frac{1}{N} C_{J_{\mathbf{k}(-t)}\rho_{-\mathbf{k}}}(t) = \frac{1}{N}\langle J_{\mathbf{k}(-t)}(t)\delta\rho_{\mathbf{k}}^*(0)\rangle. \quad (2.38)$$

Then, Eq. (2.26) can be rewritten as

$$\frac{dF(\mathbf{k},t)}{dt} = -ik(-t)H(\mathbf{k},t),$$

$$\frac{dH(\mathbf{k},t)}{dt} = -\hat{\mathbf{k}}(-t)\cdot\mathbf{\Gamma}\cdot\hat{\mathbf{k}}(-t)H(\mathbf{k},t) - \frac{ik(-t)}{m\beta S(k(-t))}F(\mathbf{k},t)$$

$$- \frac{\zeta_0}{m}H(\mathbf{k},t) - \frac{1}{m}\int_0^t dt'\; \delta\zeta(\mathbf{k}(-t),t-t')H(\mathbf{k},t').$$

$$(2.39)$$

Note that in the above equation, the differential operator $\mathbf{k}\cdot\mathbf{\Gamma}\cdot\partial/\partial\mathbf{k}$ disappears because

$$\frac{dF(\mathbf{k},t)}{dt} = \frac{\partial F(\mathbf{k},t)}{\partial t} - \mathbf{k}(-t)\cdot\mathbf{\Gamma}\cdot\frac{\partial}{\partial\mathbf{k}(-t)}F(\mathbf{k},t). \quad (2.40)$$

The memory kernel Eq. (2.37) appearing in Eq. (2.39) contains the nonlinear coupling with the correlation function itself and therefore the equation should be solved self-consistently. Indrani and Ramaswamy have derived an equation similar to Eq. (2.39) for the velocity correlations of a single tagged particle in a three-dimensional hard sphere colloidal suspension [18]. They were interested in the relatively low density regime, and did not solve the resulting equation self-consistently.

For colloidal suspensions the relaxation time of the momentum fluctuations is of the order of $\tau_m = m/\zeta_0$ and is much shorter than the relaxation time for density fluctuations which is of the order of or longer than $\tau_d = \sigma^2/D_0$. In other words, we may invoke the overdamped limit. Thus, we neglect the inertial term $dH(\mathbf{k},t)/dt$. Likewise the first term of the right-hand side in the second equation of Eq. (2.39) is estimated to be of order of $\dot{\gamma}\tau_m$ and thus should be very small as long as the Péclet number is small. Thus, the equation for the momentum fluctuations may be written as

$$0 = -\frac{ik(-t)}{m\beta S(k(-t))}F(\mathbf{k},t) - \frac{\zeta_0}{m}H(\mathbf{k},t) - \frac{1}{m}\int_0^t dt'\; \delta\zeta(\mathbf{k}(-t),t$$

$$-t')H(\mathbf{k},t'). \quad (2.41)$$

Substituting this back into the first equation of Eq. (2.39), we arrive at the equation for the intermediate scattering function

$$\frac{dF(\mathbf{k},t)}{dt} = -\frac{D_0 k(-t)^2}{S(k(-t))}F(\mathbf{k},t) - \int_0^t dt'\; M(\mathbf{k}(-t),t$$

$$-t')\frac{dF(\mathbf{k},t')}{dt'}, \quad (2.42)$$

where the memory kernel is given by

$$M(\mathbf{k},t) = \frac{D_0}{2\rho_0}\frac{k}{k(t)}\int_{\mathbf{q}} V_{\mathbf{k}}(\mathbf{q},\mathbf{k}-\mathbf{q})V_{\mathbf{k}(t)}(\mathbf{q}(t),\mathbf{k}(t)-\mathbf{q}(t))$$

$$\times F(\mathbf{k}(t)-\mathbf{q}(t),t)F(\mathbf{q}(t),t). \quad (2.43)$$

Equations (2.42) and (2.43) are the final mode-coupling expressions. We have started from the equation for both the density and the momentum fields and proceeded via the standard mode-coupling approach, taking the overdamped limit at the end. It should be possible to derive the same result starting from the diffusion equation with an interaction term which is obtained by taking the overdamped limit in Eq. (2.6). In order to arrive at the same result, however, one needs to use a different resummation scheme that involves the irreducible projection operator [38].

Equation (2.42) is a nonlinear integrodifferential equation that can be solved numerically. An efficient numerical routine to solve the mode-coupling equation is elucidated in Ref. [39]. Since our equation is not isotropic in $\mathbf{k}$ due to the presence of shear, the numerics are more involved than in the equilibrium case. We shall solve the equation by dividing the lower half plane into an $N_k \times (N_k-1)/2$ grid, where N_k is the grid number which we have chosen to be an odd number. We do not need to consider the upper half plane because it is a mirror image of the lower one. k_x, for example, is discretized as $k_{x,0}=-k_c, k_{x,1}=-k_c+\delta_k, \ldots, k_{x,N_k}=-k_c+N_k\delta_k=k_c$, where $\delta_k = 2k_c/N_k$ is the grid size and k_c is a cutoff wave vector. Any value outside the boundary $|k_x|, |k_y| > k_c$ is replaced by the value at the boundary.

III. SIMULATION METHOD

To prevent crystallization and obtain stable amorphous states via molecular dynamics (MD) simulations, we choose a model two-dimensional system composed of two different particle species 1 and 2, which interact via the soft-core potential

$$v_{ab}(r) = \epsilon(\sigma_{ab}/r)^{12} \quad (3.1)$$

with $\sigma_{ab}=(\sigma_a+\sigma_b)/2$, where r is the distance between two particles and a,b denote particle species ($\in 1,2$). We take the mass ratio to be $m_2/m_1=2$, the size ratio to be $\sigma_2/\sigma_1=1.4$, and the number of particles $N=N_1+N_2$, $N_1=N_2=5000$. Simulations are performed in the presence and absence of shear flow keeping the particle density and the temperature fixed at $n=n_1+n_2=0.8/\sigma_1^2$ ($n_1=N_1/V$, $n_2=N_2/V$) and $k_BT=0.526\epsilon$, respectively. Space and time are measured in units of σ_1 and $\tau_0=(m_1\sigma_1^2/\epsilon)^{1/2}$. The size of the unit cell is $L=118\sigma_1$. In the absence of shear, we impose microcanonical conditions and integrate Newton's equations of motion

$$\frac{d\mathbf{r}_i^a}{dt} = \frac{\mathbf{p}_i^a}{m_a}, \quad \frac{d\mathbf{p}_i^a}{dt} = \mathbf{f}_i^a \tag{3.2}$$

after very long equilibration periods so that no appreciable aging (slow equilibration) effect is detected in various quantities such as the pressure or in various time correlation functions. Here, $\mathbf{r}_i^a = (r_{xi}^a, r_{yi}^a)$ and $\mathbf{p}_i^a = (p_{xi}^a, p_{yi}^a)$ denote the position and the momentum of the ith particle of the species a, and $\mathbf{f}_i^a$ is the force acting on the ith particle of species a. In the presence of shear, by defining the momentum $\mathbf{p}_i'^a = \mathbf{p}_i^a - m_a \dot\gamma r_{yi}^a \hat{\mathbf{e}}_x$ (the momentum deviations relative to mean Couette flow), and using the Lee-Edwards boundary condition, we integrate the so-called SLLOD equations of motion so that the temperature $k_B T [\equiv N^{-1} \Sigma_a \Sigma_i (\mathbf{p}_i'^a)^2 / m_a]$ is kept at a desired value using a Gaussian constraint thermostat to eliminate viscous heating effects [40]. The system remains at rest for $t < 0$ for a long equilibration time and is then sheared for $t \geq 0$. Data for analysis have been taken and accumulated in steady states which can be realized after transient waiting periods.

We shall calculate the incoherent and the coherent parts of the scattering function for the binary mixture by using the definitions [41]

$$F_s(\mathbf{k}, t) = \frac{1}{N_a} \left\langle \sum_{i=1}^{N_a} e^{[-i\{\mathbf{k}(-t)\cdot\mathbf{r}_i^a(t) - \mathbf{k}\cdot\mathbf{r}_i^a(0)\}]} \right\rangle \tag{3.3}$$

and

$$F_{ab}(\mathbf{k}, t) = \frac{1}{N} \left\langle \sum_{i=1}^{N_a} e^{[-i\mathbf{k}(-t)\cdot\mathbf{r}_i^a(t)]} \sum_{j=1}^{N_b} e^{[i\mathbf{k}\cdot\mathbf{r}_j^b(0)]} \right\rangle, \tag{3.4}$$

respectively, with $a, b \in 1, 2$. The α relaxation time τ_α of the present mixture, which is defined by

$$F_{11}(\mathbf{k}_0, \tau_\alpha) \simeq F_s(\mathbf{k}_0, \tau_\alpha) = e^{-1}, \tag{3.5}$$

is equal to $\tau_\alpha \simeq 1800$ time units in the quiescent state for $|\mathbf{k}_0| = 2\pi/\sigma_1$.

IV. RESULTS

A. Microscopic structure

The partial static structure factors $S_{ab}(\mathbf{k})$ are defined as

$$S_{ab}(\mathbf{k}) = \int d\mathbf{r} \, e^{i\mathbf{k}\cdot\mathbf{r}} \langle \hat{n}_a(\mathbf{r}) \hat{n}_b(0) \rangle, \tag{4.1}$$

where

$$\hat{n}_a(\mathbf{r}) = \sum_j^{N_a} \delta(\mathbf{r} - \mathbf{r}_j^a) \ (a = 1, 2) \tag{4.2}$$

is the local number density of the species a. Note the dimensionless wave vector $\mathbf{k}$ is measured in units of σ_1^{-1}. For a binary mixture there are three combinations of partial structure factors $S_{11}(\mathbf{k})$, $S_{22}(\mathbf{k})$, and $S_{12}(\mathbf{k})$. They are plotted in Fig. 2(a) in the quiescent state after taking an angular average over $\mathbf{k}$. A density variable representing the degree of particle packing, corresponding to the density of an effective
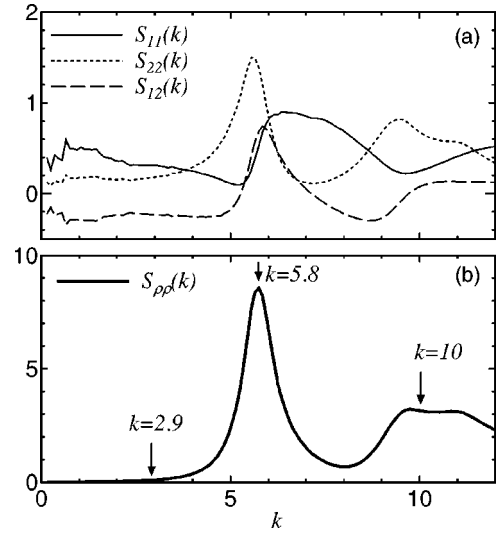

FIG. 2. Partial structure factors $S_{ab}(k)$ in (a) and $S_{\rho\rho}(k)$ in (b) defined by Eq. (4.4) for the present binary mixture.

one component system, can be defined for the present binary system by

$$\hat{\rho}_{\text{eff}}(\mathbf{r}) = \sigma_1^2 \hat{n}_1(\mathbf{r}) + \sigma_2^2 \hat{n}_2(\mathbf{r}). \tag{4.3}$$

The corresponding dimensionless structure factor is given by

$$S_{\rho\rho}(\mathbf{k}) = \sigma_1^{-4} \int d\mathbf{r} \, e^{i\mathbf{k}\cdot\mathbf{r}} \langle \delta\hat{\rho}_{\text{eff}}(\mathbf{r}) \delta\hat{\rho}_{\text{eff}}(0) \rangle = n_1^2 S_{11}(\mathbf{k})$$
$$+ n_2^2 (\sigma_2/\sigma_1)^4 S_{22}(\mathbf{k}) + 2 n_1 n_2 (\sigma_2/\sigma_1)^2 S_{12}(\mathbf{k}), \tag{4.4}$$

where $\delta\hat{\rho}_{\text{eff}} = \hat{\rho}_{\text{eff}} - \langle \hat{\rho}_{\text{eff}} \rangle$. One can see from Fig. 2(b) that $S_{\rho\rho}(k)$ has a pronounced peak at $k \simeq 5.8$ and becomes very small (~ 0.01) at smaller k demonstrating that our system is highly incompressible at long wavelengths. Because $S_{\rho\rho}(k)$ behaves quite similarly to $S(k)$ of one component systems, we examine space-time correlations in $\hat{\rho}_{\text{eff}}(\mathbf{r})$ rather than those in the partial number density $\hat{n}_a(\mathbf{r})$ for the present binary system. The usage of $\hat{\rho}_{\text{eff}}(\mathbf{r})$ makes comparisons of our simulation data with the mode-coupling theory developed for a one component system more meaningful.

We next examine the anisotropy in the static structure factor $S_{\rho\rho}(\mathbf{k})$ in the presence of shear flow. Figures 3–6 show $S_{\rho\rho}(\mathbf{k})$ plotted on a two-dimensional k_x-k_y plane (upper part) and the angular averaged curves (lower part) within the regions (a)–(d) obtained at $\dot\gamma = 10^{-4}$, 10^{-3}, 10^{-2}, and 10^{-1}, respectively (in units of τ_0^{-1}). One sees that, at the lowest shear rate ($\dot\gamma = 10^{-4}$), the shear distortion is negligible but at higher shear rate the distortion becomes prominent. At $\dot\gamma = 10^{-3}$, at all regions except for the region (d), the peak heights of $S_{\rho\rho}(\mathbf{k})$ start decreasing. This is contrary to the estimate from the linear response theory given by Eq. (2.5) which predicts no distortion in the regions (a) and (c) but distortion to the higher (b) and lower (d) peaks. This seems to indicate that the nonlinear effects due to the shear become important. Ronis has explored the higher shear regime for the structure factor of hard sphere colloidal suspensions and concluded
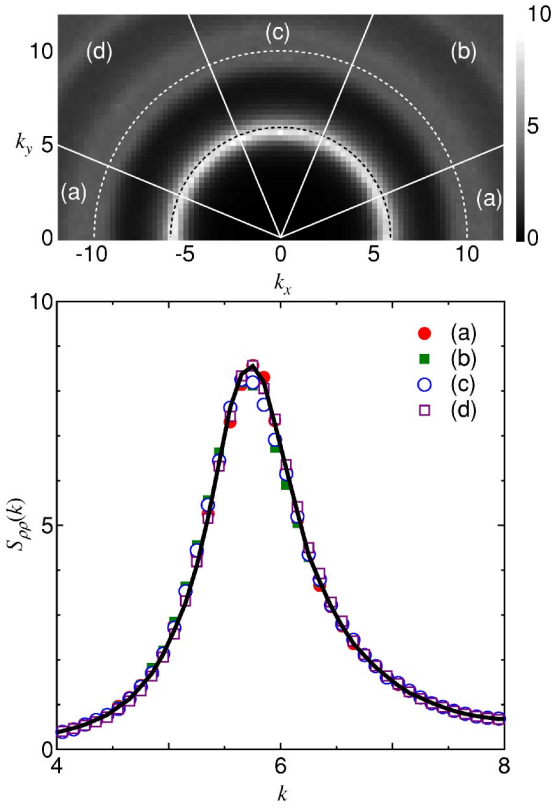
FIG. 3. $S_{\rho\rho}(k)$ for $\dot{\gamma}=10^{-4}$. The solid line is $S_{\rho\rho}(k)$ at equilibrium. Dots represent those observed in the region indicated in the (k_x, k_y) plane above.

FIG. 4. $S_{\rho\rho}(k)$ for $\dot{\gamma}=10^{-3}$. All symbols are as in Fig. 3.

that at higher shear, the peak should always be lower than the equilibrium value together with a shift that depends on the direction [25]. Figure 6 shows that peaks in all directions have been lowered and the peak with maximal distortion [region (b)] is shifted to the lower wave vectors while the opposite is true for the shift of the region with minimal distortion [region (d)]. The qualitative agreement with Ronis' theory is good but it is not clear that our results can be explained by a simple two-body theory such as that of Ronis. Recently Szamel has analyzed $S(k)$ for hard sphere colloidal suspensions up to the linear order in $\dot{\gamma}$ [42]. He took the three-body correlations into account and found quantitative agreement with the shear viscosity evaluated using $S(k)$.

It should be noted that because our system is a liquid, we cannot directly refer to the Péclet number since the bare diffusion coefficient D_0 does not exist. Therefore, a direct and quantitative comparison with the theories discussed above is not possible. However, estimates from the relaxation times self-diffusion coefficient evaluated in Ref. [6] allow us to estimate a Péclet number in the range between 10^{-1} and 10^2, which corresponds to the highest shear rates explored in the theoretical analysis of this paper.

B. Intermediate scattering function: Numerical results

Here, we examine the dynamics of the local density variable $\hat{\rho}_{\text{eff}}(\mathbf{r}, t)$. To this end, we defined the intermediate scattering function
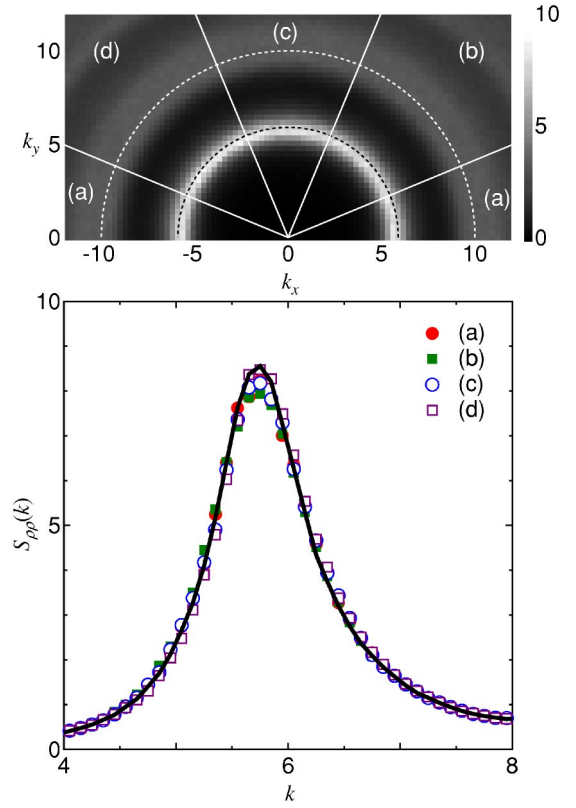
$$F_{\rho\rho}(\mathbf{k}, t) = n_1^2 F_{11}(\mathbf{k}, t) + n_2^2 (\sigma_2/\sigma_1)^4 F_{22}(\mathbf{k}, t)$$
$$+ 2n_1 n_2 (\sigma_2/\sigma_1)^2 F_{12}(\mathbf{k}, t) \quad (4.5)$$

by taking a linear combination of the partial scattering functions defined in Eq. (3.4). Note that $F_{\rho\rho}(\mathbf{k}, 0) = S_{\rho\rho}(\mathbf{k})$ by definition. To investigate anisotropy in the scattering function $F_{\rho\rho}(\mathbf{k}, t)$, the wave vector $\mathbf{k}$ is taken in four different directions $\mathbf{k}_{10}$, $\mathbf{k}_{11}$, $\mathbf{k}_{01}$, and $\mathbf{k}_{-11}$, where

$$\mathbf{k}_{\mu\nu} = \frac{k}{\sqrt{\mu^2 + \nu^2}} (\mu \hat{\mathbf{e}}_x + \nu \hat{\mathbf{e}}_y) \quad (4.6)$$

and $\mu, \nu \in 0, 1$ as shown in Fig. 7. The wave vector k (in reduced units) is taken to be 2.9, 5.8, and 10 [see also Fig. 2(b)]. Because we use the Lee-Edwards periodic boundary condition, the available wave vectors in our simulations should be given by

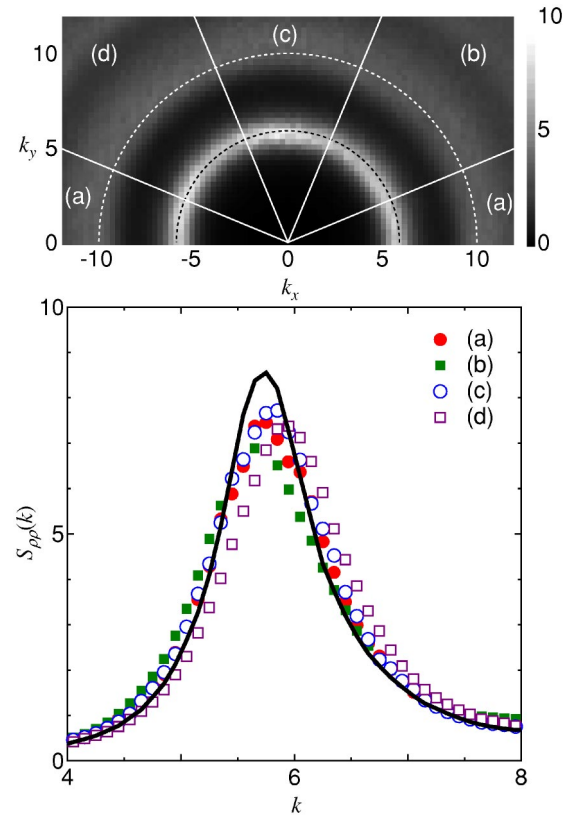$$\mathbf{k} = \frac{2\pi}{L} [n \hat{\mathbf{e}}_x, (m - nD_x) \hat{\mathbf{e}}_y], \quad (4.7)$$

where n and m are integers, $D_x = L\dot{\gamma}t$ is the difference in the x coordinate between the top and bottom cells as depicted in Fig. 6.5 of Ref. [40]. To suppress statistical errors, we sample about 80 available wave vectors around $\mathbf{k}_{\mu\nu}$ and calculate $F_{\rho\rho}(\mathbf{k}, t)$ using Eqs. (4.5) and (3.4), and then we average $F_{\rho\rho}(\mathbf{k}, t)$ over sampled wave vectors. The sampled wave vectors are shown as the spots in Fig. 7.
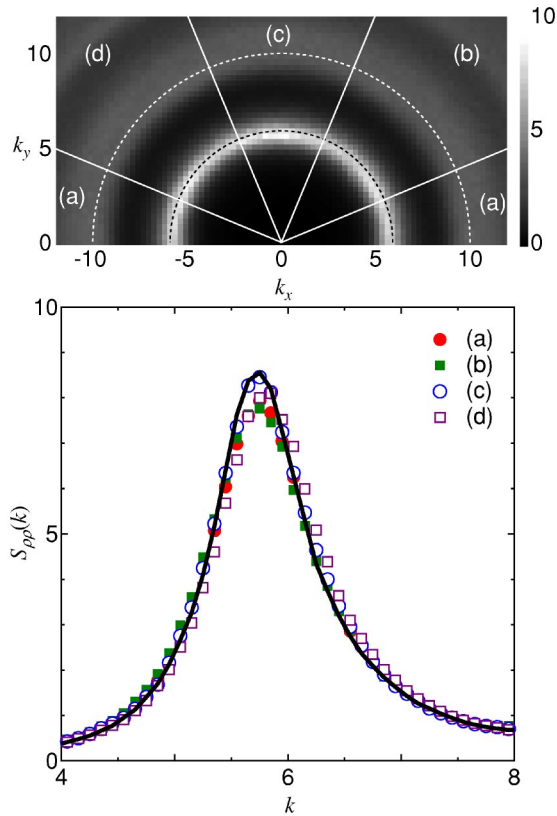
FIG. 5. $S_{\rho\rho}(k)$ for $\dot{\gamma}=10^{-2}$. All symbols are as in Fig. 3.

FIG. 6. $S_{\rho\rho}(k)$ for $\dot{\gamma}=10^{-1}$. All symbols are as in Fig. 3.

Figures 8–10 show $F_{\rho\rho}(\mathbf{k},t)/S_{\rho\rho}(\mathbf{k})$ for $k=2.9$, 5.8, and 10, respectively. We have observed that all of the partial scattering functions $F_{11}(\mathbf{k},t)$, $F_{12}(\mathbf{k},t)$, and $F_{22}(\mathbf{k},t)$ behave in a similar manner as $F_{\rho\rho}(\mathbf{k},t)$, which demonstrates that the effective single component scattering function typifies the dynamics of the whole system. Several features are noticeable. First, the quantitative trends as a function of k are similar for different values of $\dot{\gamma}$. Secondly, shear drastically accelerates microscopic structural relaxation in the supercooled state. The structural relaxation time τ_α decreases strongly with increasing shear rate as $\tau_\alpha \sim \dot{\gamma}^{-\nu}$ with $\nu \simeq 1$. Lastly, the acceleration in the dynamics due to shear occurs almost isotropically. We observed surprisingly small anisotropy in the scattering functions even under extremely strong shear $\dot{\gamma}\tau_\alpha \simeq 10^3$. A similar isotropy in the tagged particle motions has already been reported in Ref. [6]. The observed isotropy is more surprising than that observed in single particle quantities. In particular, the fact that different particles labels are correlated in the collective quantity defined in Eq. (3.4) means that a simple transformation to a frame moving with the shear flow cannot completely remove the directional character of the shear. Our results provide *post facto* justification for the isotropic approximation of Ref. [17]. This simplicity in the dynamics is quite different from behavior of other complex fluids such as critical fluids or polymers, where the dynamics become noticeably anisotropic in the presence of shear flow.

C. Intermediate scattering function: MCT results

We evaluate $F(k,t)$ for the two-dimensional colloidal suspension theoretically using Eq. (2.42) with Eq. (2.43). Fol-
lowing the procedure explained in Sec. II, we have solved Eq. (2.42) self-consistently. For the static correlation function $c(k)$ and $S(k)$, the analytic expressions derived by Baus *et al.* were used (see the Appendix) [43]. The number of grid points was chosen to be $N_k=55$. We have also calculated solution of Eq. (2.42) for the larger grid sizes up to $N_k =101$ but qualitative differences between results obtained with different grid numbers were not noticeable. We chose $k_c\sigma=10\pi$ as the cutoff wave vector. The best estimate for the
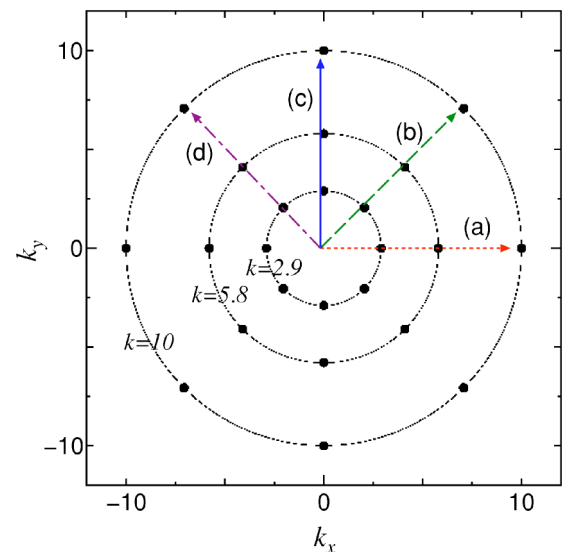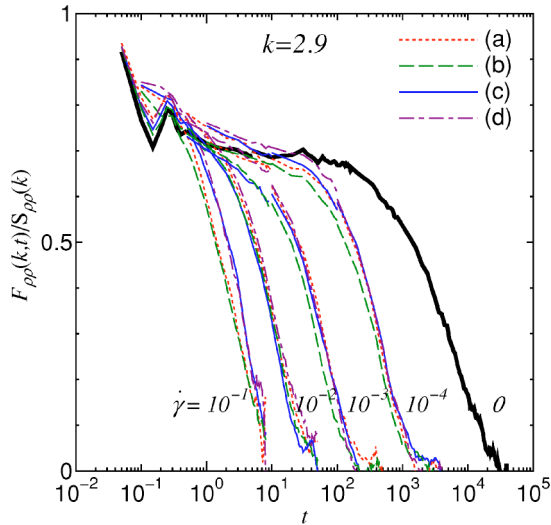

FIG. 7. Sampled wave vectors.

FIG. 8. $F(\mathbf{k},t)/S(\mathbf{k})$ at $k\sigma_1=2.8$ for various shear rates and at the different observing points (a) $\mathbf{k}_{10}$, (b) $\mathbf{k}_{11}$, (c) $\mathbf{k}_{01}$, and (d) $\mathbf{k}_{-11}$ as explained in Fig. 7.

transition density is $\phi_c=0.72574$ for $N_k=670$ at equilibrium, where $\phi=\pi\sigma^2\rho_0/4$ is the volume fraction. For $N_k=55$, a higher value, $\phi_c=0.76645$ is obtained. Figures 11–13 show the behavior of $F(\mathbf{k},t)$ renormalized by its initial value $S(k)$ for $\phi=\phi_c\times(1-10^{-4})$ for various shear rates from $Pe=10^{-10}$ to 10^{-1}, where Pe is the Péclet number defined by $Pe=\dot{\gamma}\sigma^2/D_0$. The wave vectors were chosen to be $k\sigma=3.0$ (Fig. 11), $k\sigma=6.7$ (Fig. 12), and $k\sigma=12.0$ (Fig. 13). $k\sigma=6.7$ is close to the position of the first peak of $S(k)$. At each wave vector, we have observed $F(\mathbf{k},t)/S(k)$ for four directions denoted by (a)–(d) in Fig. 7 and defined by Eq. (4.6). For shear rates smaller than $Pe=10^{-10}$ no effect of shear is observed. For $Pe\geq10^{-10}$, we observe a large reduction of relaxation times due to shear. We define the structural relaxation time τ_α as in Eq. (3.5). We find that, although the amplitudes of relaxation defer depending on k, the shear dependence of the relaxation time and its shear dependence is almost indepen-
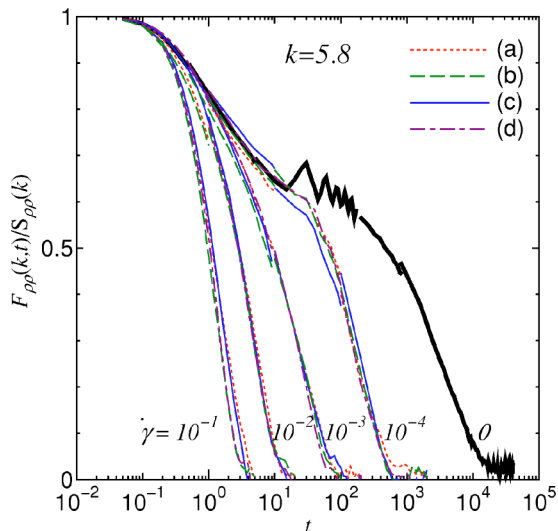

FIG. 9. $F(\mathbf{k},t)/S(\mathbf{k})$ at $k\sigma_1=5.8$. All symbols are as in Fig. 8.
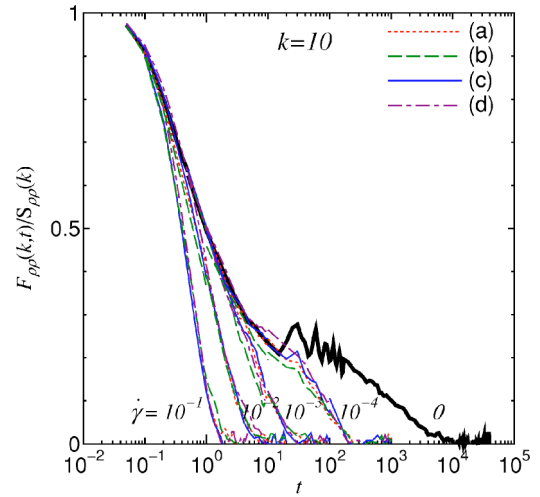

FIG. 10. $F(\mathbf{k},t)/S(\mathbf{k})$ at $k\sigma_1=10$. All symbols are as in Fig. 8.

dent of k. The shear rate dependence of the relaxation time is given by $\tau_\alpha(\dot{\gamma})\sim\dot{\gamma}^{-1}$, consistent with the simulation results discussed in the previous subsection. The four curves for a fixed shear rate but for different wave vector directions exhibit almost perfect isotropy, in qualitative agreement with the behavior observed in the simulations. Thus the apparent anisotropy of the vertex function in Eq. (2.43) provides virtually no anisotropic scattering. For $k\sigma=3$, we see perfectly isotropic scattering. For $k\sigma=6.7$ and 12.0, the curves show small anisotropy that is still consistent with the simulation results. Note that the differences shown in the plateau value for $k\sigma=12.0$ is an artifact due to our use of a square grid which produces an error in the radial distances depending on direction. The differences are noticeable but small in (b) and (d) for $k\sigma=12.0$. In these calculations, we have used the
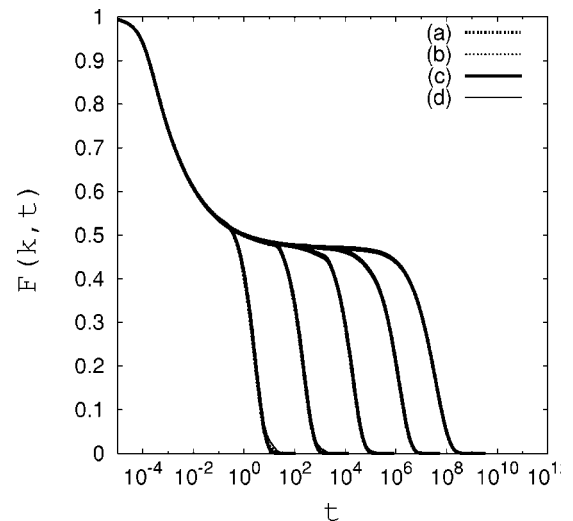

FIG. 11. $F(\mathbf{k},t)/S(k)$ for $k\sigma=3$ for different observing points and for various shear rates. From the right to the left, $Pe=10^{-10}$, 10^{-7}, 10^{-5}, 10^{-3}, and 10^{-1}. The thick dotted lines are at (a) in Fig. 7. The thin dotted lines are at (b). The thick solid lines are at (c). The thin solid lines are at (d). The density is $\phi=\phi_c\times(1-10^{-4})$. The time t is scaled by σ^2/D_0.
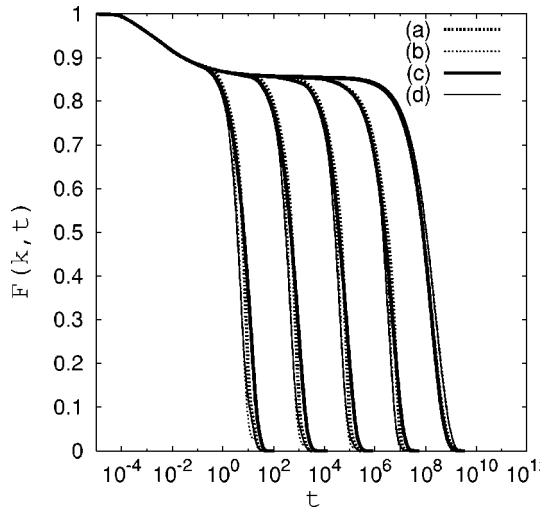
FIG. 12. $F(\mathbf{k},t)/S(k)$ for $k\sigma=6.7$. All symbols are as in Fig. 11.

FIG. 14. The reduced viscosity, (4.9), versus the shear rate for various densities. Here $Pe=\dot{\gamma}\sigma^2/D_0$. From top to bottom; ϕ $=0.766549$, 0.76650, 0.766453, 0.76640, 0.76600, and 0.75600. The highest density is $4\times10^{-5}\%$ larger than ϕ_c.

static structure factor at equilibrium and the distortion of the structure due to the shear was neglected. However, as shown in Figs. 3–6, the shape of $S(k)$ becomes weakly anisotropic under shear. In order to see if the anisotropy of the structures affects the dynamics, we have implemented the same MCT calculation using $S(k)$ and $nc(k)$ with an anisotropic sinusoidal modulation mimicking those observed in the simulations. We found that, as long as modulations are small, no qualitative change was observed and the dynamics was still isotropic.

It is surprising that, although the perturbation is highly anisotropic, the dynamics of fluctuations are almost isotropic. The reason for the isotropic nature of fluctuations may be understood as follows: The shear flow perturbs and randomizes the phase of coupling between different modes. This perturbation dissipates the cage that transiently immobilizes particles. Mathematically, this is reflected through the time dependence of the vertex. This "phase randomization" occurs irrespective of the direction of the wave vector, which results
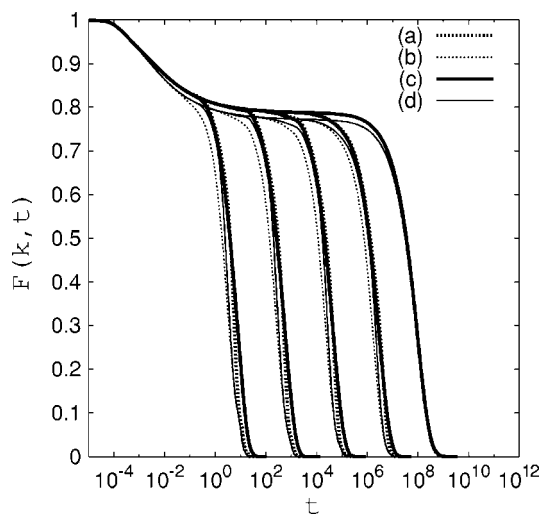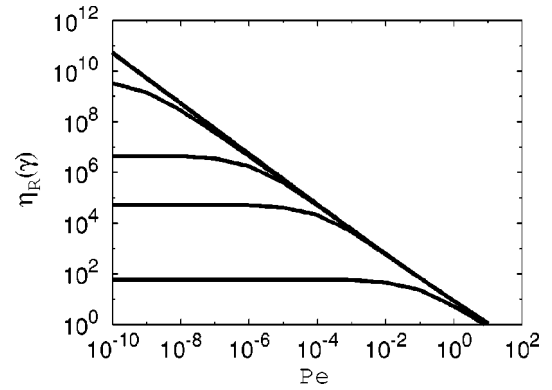
in the essentially isotropic behavior of relaxation. This mechanism is different from that of many complex fluids and of dynamics near a critical point under shear, in which anisotropic distortion of the fluctuations at small wave vectors by shear plays an essential role [37].

D. Viscosity

The shear-dependent viscosity $\eta(\dot{\gamma})$ is evaluated by modifying the mode-coupling expression for the viscosity near equilibrium [44]. This can be done by following the same procedure explained in Sec. II for the total momentum both from solvent molecules and colloids. The equation for the total momentum is given by the Navier-Stokes equation. The nonlinear term in the equation comes from the osmotic pressure of the suspension particles. Neglecting the coupling of the density field of colloids with that of the solvent molecules, one obtains the mode-coupling expression for the viscosity. In the presence of the shear, the same modification as in Eq. (2.37) is necessary and the wave vectors should be replaced by their time-dependent counterparts. The final result is given by

$$\eta(\dot{\gamma}) = \eta_0 + \frac{1}{2\beta} \times \int_0^{\infty} dt \int \frac{d\mathbf{k}}{(2\pi)^2}$$

$$\times \frac{k_x k_x(t)}{S^2(k)S^2(k(t))} \frac{\partial S(k)}{\partial k_y} \frac{\partial S(k(t))}{\partial k_y(t)} F^2(\mathbf{k}(t),t), \quad (4.8)$$

where η_0 is the viscosity of the solvent alone. The integral over $\mathbf{k}$ can be implemented for the set of $F(k,t)$ evaluated using Eq. (2.42). In Fig. 14, we have plotted the shear dependence of the reduced viscosity defined by

$$\eta_R(\dot{\gamma}) \equiv \frac{\eta(\dot{\gamma}) - \eta_0}{\eta_0} \quad (4.9)$$

for various densities around ϕ_c. The strong non-Newtonian behavior is observed at high shear rate and large densities, which is again in qualitative agreement with the simulation results for liquids reported in Ref. [6]. The shear thinning exponent extracted from the data between $10^{-10}<Pe<1$ is

FIG. 13. $F(\mathbf{k},t)/S(k)$ for $k\sigma=12$. All symbols are as in Fig. 11.

$\eta_R(\dot{\gamma}) \propto \dot{\gamma}^{-\nu}$ with $\nu \simeq 0.99$. This is in agreement with the exponent estimated from the simulation results and the structural relaxation time $\tau_\alpha(\dot{\gamma})$ observed in the simulation and in the theory discussed in the previous subsections. For larger shear rates, Pe > 1, the exponent becomes smaller, which is again consistent with computer simulation [6]. However, one should not trust this reasoning for Pe > 1. As discussed in Sec. IV A, it is expected that the distortion of structure $c(k)$ and $S(k)$ by shear becomes important and one should take these effects into account in the theory. In this regime, however, the glassy structure has already been destroyed and the system becomes more similar to a "liquid." In the liquid state, the shear-thinning exponent is always expected to be smaller than 1 and range between 0.5 and 0.8 [3,4,7,45].

Slightly above ϕ_c, plastic behavior is observed, which implies the presence of the yield stress. Note that this is an artifact of the theory because ϕ_c predicted from the mode-coupling theory is much lower than the real glass transition density. Below the real glass transition density ϕ_g, it is expected that shear thinning behavior similar to that predicted by MCT for $\phi < \phi_c$ will result.

V. CONCLUSIONS

In this paper, we presented the derivation of the mode-coupling equation for the *realistic* supercooled fluids under shear and compared the results with the molecular dynamic simulation. Our starting point is fluctuating hydrodynamics extended to the molecular length scales. A simple closed equation for the intermediate scattering function was derived. We applied the theory to a two-dimensional colloidal suspension with hard-core interactions. The numerical analysis of the equation revealed very good agreement with simulation results for a related system: a binary liquid interacting with a soft-core potential. Theory and simulation showed common features such as (i) drastic reduction of relaxation times and the viscosity and (ii) nearly isotropic relaxation irrespective of the direction of the shear flow. The fact that the dynamics is almost isotropic supports the validity of the schematic models proposed so far, in which the anisotropic nature of the nonequilibrium states was not explicitly considered [14,17].

The mode-coupling theory developed in this paper is far from complete. The most crucial approximation is the use of the first FDT, which was employed when we close the equation for dynamical correlators. It is already known that the first FDT is violated for supercooled systems under shear as well as aging systems [7]. Without the first FDT, one has to solve simultaneously the set of mode-coupling equations for the propagator and correlation function, which couple each other through the memory kernels. Research in this direction is under way. A simple argument, however, should suffice to explain the success of the present theory with regard to shear thinning behavior. Consider a system that evolves out of equilibrium with one effective temperature T_{eff}. Crudely, we can use the effective steady state version of FDT violation in the form

$$\chi_{ij}(t) = -\frac{\theta(t)}{k_B T_{\text{eff}}} \frac{dC_{ij}(t)}{dt} \tag{5.1}$$

to eliminate the response function $\chi_{ij}(t)$ in favor of the correlation function $C_{ij}(t)$ from the set of mode-coupling equa-

tions. We thus expect for the behavior of the structural relaxation time $\tau_\alpha(\dot{\gamma})$ will be unaffected as long as Eq. (5.1) holds. Another important approximation was to neglect the small distortion of the structure [$c(k)$ and $S(k)$] due to shear. The simulation supports that the distortion is negligibly small at the low shear rates (small Péclet number). The construction of the equation for equal-time correlation functions such as the structure factor might be more subtle and should be considered in future. Simulation results show that the structure is distorted in a noticeable and anisotropic manner at high shear rates; the peak height of the first peak of $S(k)$ was lowered as much as 10% at $\dot{\gamma} = 10^{-1}$. It is interesting that the dynamics is still isotropic and qualitative behavior is not affected even for such high shear rates.

In the absence of shear, MCT is known to break down at densities well below the real glass-transition density, where MCT incorrectly predicts a fictitious nonergodic transition. Beyond this MCT crossover density, activated hopping between the local minima of the free energy surface is expected to dominate the dynamics of the system. Sollich *et al.* [46,47] have analyzed a schematic model for hopping processes and explained similar shear thinning behavior. Lacks [48] has also rationalized shear thinning behavior in terms of changes of the free energy barriers due to shear. It is interesting that the totally different picture given by MCT leads to some qualitatively similar conclusions. The analysis of the violation of the first FDT and effective temperatures has the possibility of clarifying the difference between these distinct pictures. Barrat *et al.* have shown by simulation that the first FDT is violated in a sheared liquid and observed nontrivial effective temperatures [7]. This is consistent with the conclusion of Berthier *et al.* [14] for the nonequilibrium *p*-spin model. On the other hand, the trap model predicts multiple effective temperatures [47]. Future effort will be directed towards extracting effective temperatures from our fluctuating hydrodynamic approach.

In Sec. II we have mentioned that there are subtle problems in constructing an equation for the intermediate scattering function alone: The "correct" MCT equation can be derived if you start from the nonlinear Langevin equations for the density and momentum fields, taking the overdamped limit at the end. But difficulties arise if the overdamped limit is taken for the Langevin equation at the beginning. These problems exist even for systems at equilibrium and are related to generic problems that exist in loop expansion methods. These subtleties were already recognized in the mid 1970's [34] and recently pointed out in the context of glassy systems by Schmitz *et al.* [49]. A detailed study of these and issues related to the field-theoretic approach to out-of-equilibrium glassy liquids will be discussed in a future publication [32].

APPENDIX: STATIC STRUCTURE FOR THE TWO-DIMENSIONAL FLUIDS WITH THE HARD-CORE INTERACTION

Baus *et al.* have derived an approximated analytic expression of the direct correlation function $c(k)$ for the d-dimensional hard sphere fluids [43]. For the two-dimensional system, it is given by

$$
nc(k) = -\phi \frac{\partial \{\phi Z(\phi)\}}{\partial \phi} \left[4(1 - a^2 \phi) f(k\sigma) \right.
$$
$$
\left. + a^2 \phi \left\{ a^2 \left(\frac{J_1(ak\sigma/2)}{ak\sigma/2} \right)^2 + \frac{16}{\pi} \int_{1/a}^1 dx \, (1 \right. \right.
$$
$$
\left. \left. - x^2)^{1/2} \left(\frac{J_1(k\sigma)}{k\sigma} - (ax)^2 \frac{J_1(ak\sigma x)}{ak\sigma} \right) \right\} \right], \quad \text{(A1)}
$$

where $J_n(x)$ is the Bessel function of the first kind,

$\phi = \pi \sigma^2 \rho_0 / 4$ is the packing fraction, ρ_0 is the number density, and σ is the diameter of spheres. a is a parameter which is determined by solving

$$
\frac{2}{\pi} \left[a^2(a^2 - 4) \arcsin\left(\frac{1}{a}\right) - (a^2 + 2)\sqrt{a^2 - 1} \right] = \frac{1}{\phi^2} \left[1 - 4\phi \right.
$$
$$
\left. - \left\{ \frac{\partial \{\phi Z(\phi)\}}{\partial \phi} \right\}^{-1} \right]. \quad \text{(A2)}
$$

$Z(\phi) \equiv p/\rho_0 k_B T$ is the compressibility factor which is expanded by a rescaled virial series as

$$
Z(\phi) = (1 - \phi)^{-2} \left(1 + \sum_{n=1}^{\infty} c_n \phi^n \right), \quad \text{(A3)}
$$

where c_n is a coefficient which is related to the virial coefficients via a recurrence relation. We truncated the series at $n = 6$. The coefficients c_n are given by $c_1 = 0$, $c_2 = 0.1280$, $c_3 = 0.0018$, $c_4 = -0.0507$, $c_5 = -0.0533$, and $c_6 = -0.0410$.

[1] R. G. Larson, *The Structure and Rheology of Complex Fluids* (Oxford University Press, Oxford, 1999).

[2] M. Doi and S. F . Edwards, *The Theory of Polymer Dynamics* (Oxford University Press, Oxford, 1986).

[3] T. Naitoh and S. Oono, Phys. Lett. **57A**, 448 (1976).

[4] T. R. Kirkpatrick, J. Non-Cryst. Solids **75**, 437 (1985).

[5] J. H. Simmons, R. K. Mohr, and C. J. Montrose, J. Appl. Phys. **53**, 4075 (1982); J. H. Simmons, R. Ochoa, and K. D. Simmons, J. Non-Cryst. Solids **105**, 313 (1988); Y. Yue and R. Brückner, *ibid.* **180**, 66 (1994).

[6] R. Yamamoto and A. Onuki, Phys. Rev. E **58**, 3515 (1998).

[7] J.-L. Barrat and L. Berthier, Phys. Rev. E **63**, 012503 (2000); L. Berthier and J.-L. Barrat, Phys. Rev. Lett. **89**, 095702 (2002); L. Berthier and J.-L. Barrat, J. Chem. Phys. **116**, 6228 (2002).

[8] L. Angelani, G. Ruocco, F. Sciortino, P. Tartaglia, and F. Zamponi, Phys. Rev. E **66**, 061505 (2002).

[9] R. Yamamoto and A. Onuki, J. Chem. Phys. **117**, 2359 (2002).

[10] A. J. Liu and S. R. Nagel, Nature (London) **396**, 21 (1998).

[11] L. F. Cugliandolo, in *Slow Relaxations and Nonequilibrium Dynamics in Condensed Matter*, edited by J.-L. Barrat, M. Feigelman, and J. Kurchan (Springer-Verlag, New York, 2003), pp. 371–521.

[12] W. Kob, J.-L. Barrat, F. Sciortino, and P. Tartaglia, J. Phys.: Condens. Matter **12**, 6385 (2000).

[13] A. Latz, J. Phys.: Condens. Matter **12**, 6353 (2000); A. Latz, J. Stat. Phys. **109**, 607 (2002).

[14] L. Berthier, J.-L. Barrat, and J. Kurchan, Phys. Rev. E **61**, 5464 (2000).

[15] V. Viasnoff and F. Lequeux, Phys. Rev. Lett. **89**, 065701 (2002).

[16] K. Miyazaki and D. R. Reichman, Phys. Rev. E **66**, 050501(R) (2002).

[17] M. Fuchs and M. E. Cates, Phys. Rev. Lett. **89**, 248304 (2002); M. Fuchs and M. E. Cates, J. Phys.: Condens. Matter **15**, S401 (2003); M. Fuchs and M. E. Cates, Faraday Discuss.

123, 267 (2003).

[18] A. V. Indrani and S. Ramaswamy, Phys. Rev. E **52**, 6492 (1995).

[19] S. P. Das, G. F. Mazenko, S. Ramaswamy, and J. J. Toner, Phys. Rev. Lett. **54**, 118 (1985); S. P. Das and G. F. Mazenko, Phys. Rev. A **34**, 2265 (1986).

[20] T. R. Kirkpatrick and J. C. Nieuwoudt, Phys. Rev. A **33**, 2651 (1986); **33**, 2658 (1986).

[21] L. D. Landau and E. M. Lifshitz, *Fluid Mechanics* (Pergamon, New York, 1959).

[22] C. W. J. Beenakker and P. Mazur, Physica A **126**, 349 (1984).

[23] The name of "the first" and "the second" FDT are from the textbook of Kubo [50].

[24] F. Sciortino and W. Kob, Phys. Rev. Lett. **86**, 648 (2001).

[25] D. Ronis, Phys. Rev. A **29**, 1453 (1984).

[26] L. M. Lust, O. T. Valls, and C. Dasgupta, Phys. Rev. E **48**, 1787 (1993).

[27] W. Götze and L. Sjögren, Rep. Prog. Phys. **55**, 241 (1992).

[28] R. Zwanzig, *Nonequilibrium Statistical Mechanics* (Oxford University Press, Oxford, 2001).

[29] K. Kawasaki, Ann. Phys. (N.Y.) **61**, 1 (1970).

[30] P. C. Martin, E. D. Siggia, and H. A. Rose, Phys. Rev. A **8**, 423 (1973).

[31] R. Phythian, J. Phys. A **10**, 777 (1977).

[32] K. Miyazaki and D. R. Reichman (unpublished).

[33] S.-k. Ma and G. F. Mazenko, Phys. Rev. B **11**, 4077 (1975).

[34] U. Deker and F. Haake, Phys. Rev. A **11**, 2043 (1975).

[35] J.-P. Bouchaud, L. Cugliandolo, J. Kurchan, and M. Mézard, Physica A **226**, 243 (1996).

[36] K. Kawasaki and S. Miyazima, Z. Phys. B: Condens. Matter **103**, 423 (1997).

[37] A. Onuki, J. Phys.: Condens. Matter **9**, 6119 (1997); A. Onuki, *Phase Transition Dynamics* (Cambridge University Press, Cambridge, 2002).

[38] K. Kawasaki, Physica A **215**, 61 (1995).

[39] M. Fuchs, W. Götze, and A. Latz, J. Phys.: Condens. Matter **3**,

5047 (1991).

[40] D. J. Evans and G. P. Morriss, *Statistical Mechanics of Non-equilibrium Liquids* (Academic, New York, 1990).

[41] A similar but slightly different definition for $F_s(\mathbf{k}, t)$ was given in Ref. [6]. We, however, confirmed that the both definitions give almost identical results for the present case.

[42] G. Szamel, J. Chem. Phys. **114**, 8708 (2001).

[43] M. Baus and J. L. Colot, Phys. Rev. A **36**, 3912 (1987).

[44] A. J. Banchio, J. Bergenholtz, and G. Nägele, Phys. Rev. Lett. **82**, 1792 (1999).

[45] J. C. van der Werff, C. G. de Kruif, and J. K. G. Dhont, Physica A **160**, 205 (1989).

[46] P. Sollich, F. Lequeux, P. Hébraud, and M. E. Cates, Phys. Rev. Lett. **78**, 2020 (1997).

[47] S. M. Fielding and P. Sollich, Phys. Rev. E **67**, 011101 (2003).

[48] D. J. Lacks, Phys. Rev. Lett. **87**, 225502 (2001).

[49] R. Schmitz, J. W. Dufty, and P. De, Phys. Rev. Lett. **71**, 2066 (1993).

[50] R. Kubo, M. Toda, and N. Hashitsume, *Statistical Physics II: Nonequilibrium Statistical Mechanics* (Springer-Verlag, New York, 1978).